Thrombin increases the expression of cholesterol 25-hydroxylase in rat astrocytes after spinal cord injury

Chen Chen[1, 2, #], Huiyuan Ji[3, #], Nan Jiang[1], Yingjie Wang[2], Yue Zhou[1], Zhenjie Zhu[1], Yuming Hu[1], Yongjun Wang[2], Aihong Li[4, *], Aisong Guo[5, *]

https://doi.org/10.4103/1673-5374.357905

Date of submission: February 17, 2022

Date of decision: June 22, 2022

Date of acceptance: August 14, 2022

Date of web publication: October 11, 2022

From the Contents

Graphical Abstract

Thrombin/PAR1 promotes astrocyte CH25H expression by activating the ERK- and JNK-mediated NF-κB pathway

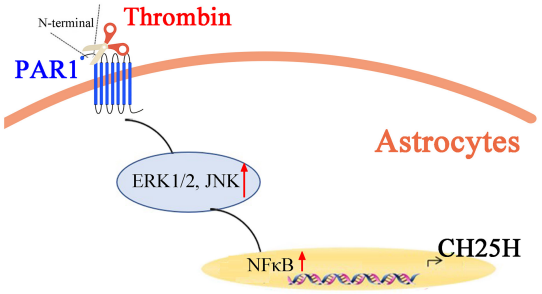

Abstract

Astrocytes are important cellular centers of cholesterol synthesis and metabolism that help maintain normal physiological function at the organism level. Spinal cord injury results in aberrant cholesterol metabolism by astrocytes and excessive production of oxysterols, which have profound effects on neuropathology. 25-Hydroxycholesterol (25-HC), the main product of the membrane-associated enzyme cholesterol-25-hydroxylase (CH25H), plays important roles in mediating neuroinflammation. However, whether the abnormal astrocyte cholesterol metabolism induced by spinal cord injury contributes to the production of 25-HC, as well as the resulting pathological effects, remain unclear. In the present study, spinal cord injury-induced activation of thrombin was found to increase astrocyte CH25H expression. A protease-activated receptor 1 inhibitor was able to attenuate this effect *in vitro* and *in vivo*. In cultured primary astrocytes, thrombin interacted with protease-activated receptor 1, mainly through activation of the mitogen-activated protein kinase/nuclear factor-kappa B signaling pathway. Conditioned culture medium from astrocytes in which *ch25h* expression had been knocked down by siRNA reduced macrophage migration. Finally, injection of the protease activated receptor 1 inhibitor SCH79797 into rat neural sheaths following spinal cord injury reduced migration of microglia/macrophages to the injured site and largely restored motor function. Our results demonstrate a novel regulatory mechanism for thrombin-regulated cholesterol metabolism in astrocytes that could be used to develop anti-inflammatory drugs to treat patients with spinal cord injury.

Key Words: 25-hydroxycholesterol; astrocyte; chemotaxis; cholesterol metabolism; cholesterol-25-hydroxylase; lipid homeostasis; macrophage; PAR1; spinal cord injury; thrombin

Introduction

An estimated 133,000 to 226,000 cases of acute spinal cord injury (SCI) occur globally every year (Lee et al., 2014). A dominant pathological feature after primary spinal cord injury (SCI) is secondary tissue damage, characterized by tissue edema, nerve cell necrosis, and inflammation, eventually leading to the formation of a spinal cavity (Ju et al., 2014; Schwab et al., 2014). The progressive neuropathology that occurs is partly attributed to disruption of the blood-spinal cord barrier, which results in infiltration of immune cells that promote ongoing damage within the lesion site microenvironment (Wang et al., 2019a). In addition, some blood-derived factors contribute to deterioration of the injury site milieu and have profound effects on cellular events within the injured spinal cord (Fu et al., 2020). If effective measures are not taken immediately after SCI, secondary tissue damage can worsen the neuropathology. Astrocytes are immediately activated following SCI, undergoing morphological, molecular, and functional changes that are collectively known as the glial reaction. The reactive astrocytes lose their ability to maintain homeostasis, and therefore switch dynamically between having detrimental or beneficial functions on spinal cord recovery (Okada et al., 2018; Yoshizaki et al., 2021). To date, however, the mechanism by which astrocytes become reactive in response to SCI has not been elucidated.

Under normal physiological condition, astrocytes perform a wide variety of essential functions in the central nervous system (CNS), including promoting development of the neural circuit, providing structural and nutrient support to the neurons, and regulating metabolite recycling (Sofroniew and Vinters, 2010; Tsai et al., 2012; Rodnight and Gottfried, 2013; Jayakumar et al., 2014). Astrocytes are also important cellular centers of lipid synthesis and metabolism, thereby contributing to CNS lipid homeostasis (Ioannou et al., 2019). Disruption of the astrocyte lipid metabolism pathway exacerbates the neuropathology of traumatic SCI and neurodegenerative brain disorders (van Deijk et al., 2017; Zhu et al., 2019). Several lines of evidence indicate that loss of astrocyte cholesterol synthesis affects neuronal development and function (Ferris et al., 2017), while aberrant lipid metabolism by astrocytes can result in the production of neurotoxic derivatives (Vaya and Schipper, 2007; Maki et al., 2009). SCI-induced neuronal necrosis leads to interrupted communication with astrocytes and a reduction in lipid transfer; thus, it is reasonable to assume that the astrocytes activate lipid metabolic pathways in response to

[1]Department of Rehabilitation Medicine, Affiliated Hospital of Nantong University, Nantong, Jiangsu Province, China; [2]Key Laboratory of Neuroregeneration of Jiangsu and Ministry of Education, Co-innovation Center of Neuroregeneration, Nantong University, Nantong, Jiangsu Province, China; [3]Department of Rehabilitation Medicine, The Second Affiliated Hospital of Nantong University, Nantong, Jiangsu Province, China; [4]Department of Neurology, Affiliated Hospital of Nantong University, Nantong, Jiangsu Province, China; [5]Department of Traditional Chinese Medicine, Affiliated Hospital of Nantong University, Nantong, Jiangsu Province, China

***Correspondence to:** Aisong Guo, MD, 15851300188@163.com; Aihong Li, MD, liaihongbox@163.com.

https://orcid.org/0000-0003-2104-0231 (Aisong Guo)

#Both authors contributed equally to this work.

Funding: *This study was supported by the National Natural Science Foundation of China, No. 81971826 (to AG); the China Postdoctoral Science Foundation, No. 2020M681689 (to YH); the Scientific Research Project of The Health Commission of Jiangsu Province, No. ZDB2020003 (to AG); and the Basic Scientific Research Projects of Nantong, No. JC2020041 (to YH).*

How to cite this article: *Chen C, Ji H, Jiang N, Wang Y, Zhou Y, Zhu Z, Hu Y, Wang Y, Li A, Guo A (2023) Thrombin increases the expression of cholesterol 25-hydroxylase in rat astrocytes after spinal cord injury. Neural Regen Res 18(6):1339-1346.*

their over-accumulation. However, the regulatory mechanism of astrocyte lipid metabolism has not yet been fully elucidated.

Oxysterol is a derivative of cholesterol that participates in several aspects of lipid metabolism (Russell, 2000). The oxysterol 25-hydroxycholesterol (25-HC) is the main product of the membrane-associated enzyme cholesterol-25-hydroxylase (CH25H), which catalyzes cholesterol by adding a second hydroxyl at position 25 (Cyster et al., 2014). 25-HC has been shown to participate in signaling pathways that regulate innate and adaptive immune responses by influencing macrophages (Castrillo et al., 2003; Wong et al., 2020), mast cells (Nunomura et al., 2010), T cells (Bensinger and Tontonoz, 2008), and B cells (Bauman et al., 2009). It also mediates the pathogenesis of chronic diseases such as Alzheimer's disease (Shibata et al., 2007) and multiple sclerosis (Forwell et al., 2016). We previously found that 25-HC was involved in macrophage migration inhibitory factor induced neuropathological progression following SCI in a rat model (Zhu et al., 2019). Whether SCI-induced disruption of astrocyte metabolism promotes 25-HC production and contributes to the resulting pathologic effects deserves further study.

Thrombin, a serine protease involved in hemostasis, is generated from blood-derived prothrombin by the combined actions of factors V and X in the presence of ionized calcium (Ca^{2+}) at the site of vascular injury (Coughlin, 2005). Also, the serine protease induces a variety of protease-activated receptor (PAR)-mediated responses in the CNS that mediate neuropathology, including microglial activation, astrogliosis, demyelination, and other neurotoxicities (Suo et al., 2002; Niego et al., 2011; Burda et al., 2013; Yoon et al., 2013; Radulovic et al., 2016). Thrombin-induced cell events result from the proteolytic activation of PARs, from which the extracellular NH_2 terminus is cleaved by the thrombin and unmasks an amino acid sequence that acts as a tethered receptor ligand to initiate intracellular signaling (Grand et al., 1996). A total of four members of the PAR family, PAR1, 2, 3, and 4 have been identified, and PAR1, 3, and 4, but not PAR2, can be activated by thrombin (Coughlin, 2000; Bae et al., 2007). PAR1 is the most abundantly expressed PAR family member in the CNS (Whetstone et al., 2017). Because injury-induced activation of thrombin is a potent lipid metabolic mediator, and astrocytes are the primary cellular source of lipids in the CNS (Citron et al., 2016), it is assumed that thrombin induces astrocytic expression of CH25H, which then influences neuropathology. In the present study, we explored dynamic changes in thrombin and CH25H expression at lesion sites following SCI in a rat model. The effects of thrombin on CH25H expression, as well as the underlying mechanisms, were investigated *in vitro* using primary cultured astrocytes. Finally, rat locomotor function was evaluated following administration of the PAR1 inhibitor SCH79797 to the lesion site of the contused cord.

Methods

Animals

Because male rats have fewer postoperative complications than females, which facilitates postoperative care (Patil et al., 2013), a total of 52 specific pathogen free adult male Sprague-Dawley rats aged 8–12 weeks, each weighing 180–220 g, from the Center of Experimental Animals, Nantong University (license No. 220196463), were used in this study. All procedures involving animals were approved by the Animal Care and Use Committee of Nantong University and the Animal Care Ethics Committee of Jiangsu Province (approval No. S20200323-217, January 1, 2021). All experiments were designed and reported according to the Animal Research: Reporting of *In Vivo* Experiments (ARRIVE) guidelines (Percie du Sert et al., 2020). The animals were housed in separate cages under a 12-hour light/dark cycle at 22 ± 2°C and 50% relative humidity. Food and water were provided *ad libitum*. Animals were sacrificed by CO_2 asphyxia. Briefly, animals were put in a box, and the CO_2 content of the container was increased gradually at a rate of 30–70% per minute until the animals were unconscious. Death was confirmed by cessation of movement and breathing, and having dilated pupils for 2 minutes, after which the CO_2 supply was interrupted.

Establishment of SCI rat model and drug treatment

The rat model of SCI was established as previously reported (Chehrehasa et al., 2014). Briefly, the animals were randomly divided into two groups (SCI + vehicle and SCI + SCH79797 groups, n = 24). All rats were anesthetized with 2% sodium pentobarbital (0.1 mL/kg, Sigma, St. Louis, MO, USA) by intraperitoneal injection. A skin incision was made from the eighth to the tenth thoracic vertebral level (T8–T10), and the paravertebral muscles were dissected, and the spinous process was removed at the ninth thoracic vertebral level (T9). Next, an IH-0400 Impactor (Precision Systems and Instrumentation, Lexington, KY, USA) was used to deliver a 150-kilodyne contusion injury from a height of 3 cm. Then, the impact rod was removed, the injury site was observed for edema and/or bleeding, and the wound was irrigated.

For drug delivery, the PAR1 inhibitor SCH79797 (R&D Systems, Shanghai, China) was fully dissolved in dimethyl sulfoxide (DMSO; Sigma) at a stock concentration of 10 mM and stored at –20°C. As the vehicle for SCH79797 contains DMSO, which is not biologically inert (Brayton, 1986), the 10 mM SCH79797 stock solution was prepared by adding 1 mg of SCH79797 to 0.225 mL of 2.2 mg/mL DMSO dissolved in 0.1 M phosphate-buffered saline (PBS).

For experimental use, the DMSO SCH79797 solution was diluted with 0.01 M PBS to a concentration of 5 mM and was slowly injected intrathecally (50 μg/kg, 4.5 μL of 5 mM SCH79797) before the incision was sutured. A vehicle control was also included for comparison purposes, which contained 0.225 mL of 2.2 mg/mL DMSO dissolved in 0.1 M PBS and was intrathecally delivered to rats at a dose of 4.5 μL. After surgery, penicillin (Sigma) was injected subcutaneously at a dose of 150 mg/kg for 1 week. The rats' bladders were squeezed by applying gentle pressure on the abdomen twice daily until spontaneous urination was restored.

Cell culture and treatment

Primary astrocytes were cultured according to previously described methods (Zhou et al., 2018). Briefly, a total of 88 newborn 1 to 2 days old Sprague-Dawley rats from the Center of Experimental Animals, Nantong University were used. All animals were anesthetized by hypothermia and sacrificed by the liquid nitrogen quick freezing method (Diesch et al., 2009; Mellor, 2010). The spinal cords of the newborn rats were removed and placed in 0.01 M PBS containing 1% penicillin-streptomycin. The spinal cord meninges were carefully peeled away using dissection tweezers and then subjected to enzymatic digestion (0.25% trypsin, 37°C, 15 minutes). After centrifugation at 160 × g for 5 minutes, the cells were suspended in Dulbecco's modified Eagle's medium (DMEM, Sigma) supplemented with 10% fetal bovine serum (Gibco, Carlsbad, CA, USA), 1% penicillin-streptomycin (Beyotime, Shanghai, China), and 1% L-glutamine (Beyotime). The cells were then seeded into a culture flask and maintained in a 37°C incubator with 5% CO_2. The medium was replaced every 3 days until the cells were 90–100% confluent. After shaking at 6.94 × g for 12–15 hours to remove non-astrocytes, the cells were used *in vitro*. The isolated astrocytes were more than 95% pure, as evaluated by immunofluorescence staining for the astrocytic marker glial fibrillary acid protein (GFAP, CST, Danvers, MA, USA) and Hoechst 33342 (a nuclear staining reagent that permeates the cell membrane and stains DNA; MCE, Shanghai, China), which was considered acceptable for subsequent experiments.

We used RAW264.7 cells as a macrophage model of innate immune cell. RAW264.7 cells were purchased from FuHeng Biology (Cat# FH0328, Shanghai, China). The cells' identity was confirmed by immunostaining with F4/80 and Hoechst 33342 before use, and the purity was greater than 95%. The cells were then suspended in DMEM containing 10% fetal bovine serum and maintained in a 37°C incubator with 5% CO_2.

To determine the effects of thrombin-induced astrocyte production of CH25H/25-HC, astrocytes were washed three times in serum-free DMEM for 5 minutes each time. Then the cells were treated with 1 U/mL thrombin (Sigma) for 24, 48, or 72 hours prior to performing the assay.

To determine the effects of the specific inhibitors Argatroban (for thrombin), SCH79797 (for PAR1), tcY-NH_2 (for PAR4), PD98059 (for extracellular regulated protein kinases, ERK), SP600125 (for c-Jun N-terminal kinase, JNK), SB203580 (for P38), or PDTC (for nuclear factor-κB, NFκB) on the thrombin-induced astrocytes production of CH25H/25-HC, the cells were treated with 1 U/mL thrombin with or without various concentrations of Argatroban (Sigma), SCH79797 (R&D systems), tcY-NH_2 (TOCRIS, Minneapolis, MN, USA), or PDTC (Beyotime), or 10 μM PD98059 (TOCRIS), 10 μM SP600125 (TOCRIS), or 10 μM SB203580 (TOCRIS) for 24 hours prior to performing the assay.

For knockdown, astrocytes were transfected with 5 μL *ch25h* small interfering RNA 1 (siRNA1; target sequence 5′-TCA CCA TCC TCG TCT TTC A-3′), *ch25h* siRNA2 (target sequence 5′-TCG CGA TGC TTC AGT GTC A-3′), *par3* siRNA1 (target sequence 5′-CCA ACA TCA TAC TCA TAA T-3′), or scrambled siRNA (target sequence 5′-GGC UCU AGA AAA GCC UAU GC-3′) with Lipofectamine™ RNAiMAX transfection reagent (Invitrogen, Carlsbad, CA, USA) for 48 hours, and then subjected to 1 U/mL thrombin for another 24 hours before being cultured in a Transwell system and then subjected to quantitative polymerase chain reaction (qPCR) assay. The interference efficiency of the siRNAs was calculated by comparing the relative expression of the target gene following cell transfection with the targeted siRNA and the scrambled siRNA.

qPCR

To detect the transcription levels of thrombin-regulated genes, total RNA was prepared with Trizol (Sigma) from cells or 1cm spinal segments surrounding the lesion sites at 0, 1, 4, and 7 days after SCI. The RNA was then reverse transcribed to complementary DNA (cDNA) using a HiScript 1st Strand cDNA Synthesis Kit (Vazyme, Nanjing, China). The cDNA was diluted 1:3 before performing qPCR assays. Cy3 was used as a marker of transfection efficiency. The primer sequences were designed and synthesized by Ribobio: *par1*, sense primer 5′-ACT TCA CCT GCG TGG TCA TCT G-3′, anti-sense primer 5′-ATG GCG GAG AAG GCG GAG AA-3′; *par3*, sense primer 5′-ATT GGT GTA CCA GCG AAC AT-3′, anti-sense primer 5′-CGT TCC CAT TGA GAT GGT AG-3′; *par4*, sense primer 5′-GTC AAC GCC TCA CCA CCA TAC T-3′, anti-sense primer 5′-GGA GCC AGC CAA TAG GAA GGT C-3′; glyceraldehyde-3-phosphate dehydrogenase (gapdh), sense primer 5′-ACA GCA ACA GGG TGG TGG AC-3′, anti-sense primer 5′-TTT GAG GGT GCA GCG AAC TT-3′. Endpoint qPCR was performed on a thermocycler with the specific primers using the following program: 94°C, 120 seconds; 98°C, 10 seconds; 58°C, 30 seconds; 68°C, 60 seconds for 30 cycles. The qPCR products were separated by electrophoresis on a 1% agarose gel, and images were captured using a gel imaging system. For qPCR, reactions were performed in a final volume of 10 μL (1 μL cDNA template and 9 μL reaction buffer containing 5 μL of 2× ChamQ Universal SYBR qPCR Master Mix, 3 μL of RNase free ddH_2O, and 0.5 μL each of anti-sense

and sense primers). Primer sequences are shown in **Table 1**. The reaction conditions were as follows: 94°C for 5 minutes, followed by 40 cycles of 94°C for 30 seconds, 60°C for 30 seconds, and 72°C for 30 seconds. Fluorescence was recorded during each annealing step. At the end of each qPCR run, data were collected automatically. Melting curve analysis confirmed the primer specificity and determined the cycle threshold (CT) fluorescence values. The data were analyzed by the $2^{-\Delta\Delta CT}$ method (Zeng et al., 2019). The mRNA expression levels were normalized to *gapdh*.

Table 1 | **Primer sequence**

Primer	Sequence
ch25h	Sense: 5′-ACG GAG CAA AGT TGC AGT TAA-3′
	Anti-sense: 5′-GGA GGA CCA CTC AGG TTA CGA-3′
cyp46a1	Sense: 5′-TAG CAT ACT GGT CTC CAT CCC-3′
	Anti-sense: 5′-CAG CTC CTT GGT TAG CCT GAT-3′
cyp27a1	Sense: 5′-CAG GGT CTC CTT AAT CAC AGC T-3′
	Anti-sense: 5′-GGG GTA GAC ACG ACA TCC AAT-3′
gapdh	Sense: 5′-ACA GCA ACA GGG TGG TGG AC-3′
	Anti-sense: 5′-TTT GAG GGT GCA GCG AAC TT-3′

Western blot assay

To assess the expression of the thrombin-activated proteins, astrocytes were washed with PBS and then lysed in radioimmunoprecipitation assay buffer containing 1 mM phenylmethanesulfonyl fluoride. Protein concentrations were measured using a bicinchoninic acid assay protein assay kit (Abcam, Shanghai, China). Equal amounts of protein were electrophoretically separated on a 10% sodium dodecyl sulfate-polyacrylamide gel electrophoresis gel (Beyotime) and then transferred onto a polyvinylidene difluoride membrane (Millipore, Billerica, MA, USA). After blocking with 5% skim milk for 1 hour, the membrane was incubated with the following primary antibodies overnight at 4°C: CH25H (rabbit, 1:500, Invitrogen, Cat# PA5-70691, RRID: AB_2689560), phosphorylated extracellular signal regulated kinase (pERK)1/2 (rabbit, 1:1000, CST, Cat# 9102S, RRID: AB_330744), extracellular signal regulated kinase (ERK)1/2 (rabbit, 1:1000, CST, Cat# 8544S, RRID: AB_11127856), phosphorylated c-Jun N-terminal kinase (pJNK; rabbit, 1:1000, CST, Cat# 9251S, RRID: AB_331659), JNK (rabbit, 1:1000, CST, Cat# 9252S, RRID: AB_2250373), phosphorylated P38 kinase (pP38; rabbit, 1:1000, CST, Cat# 8632S, RRID: AB_2797648), P38 (rabbit, 1:1000, CST, Cat# 14451S, RRID: AB_2798482), nuclear factor kappa-B (NFκB; rabbit, 1:1000, CST, Cat# 12629S, RRID: AB_2722509), and β-actin (mouse, 1:5000, CST, Cat# 3700S, RRID: AB_2242334). The membrane was subsequently washed three times with Tris-HCl buffered saline-Tween for 10 minutes each time, followed by incubation with the corresponding secondary antibody: goat-anti-rabbit horseradish peroxidase (1:1000, Beyotime, Shanghai, China, Cat# A0208, RRID: AB_2892644) or goat-anti-mouse horseradish peroxidase (1:1000, Beyotime, Cat# A0216, RRID: AB_2860575a) for 2 hours at 23 ± 2°C. Immunoreactive bands were visualized using chemiluminescence reagents (ECL kit, Tanon, Shanghai, China). The immunoblot results were analyzed using a Tanon Gel Imaging System (Tanon). β-Actin was used as an internal control.

Enzyme-linked immunosorbent assay

To assess the astrocytes levels of thrombin protein at the lesion site at 0, 1, 4, and 7 days following SCI, total protein was extracted from 1 cm spinal segments with 0.1 M PBS containing the protease inhibitor phenylmethanesulfonyl fluoride. After centrifuging at 2750 × *g* for 5–10 minutes at 2–8°C, the supernatant was subjected to thrombin enzyme-linked immunosorbent assay (ELISA) using a kit (Rat TAT ELISA Kit, Elabscience) according to the manufacturer's directions. The thrombin concentrations are expressed in ng/mg. Plates were read with a multifunctional enzyme marker (Biotek Synergy2, BioTek, Santa Clara, CA, USA) at a 450nm wavelength.

Tissue immunofluorescence

To study the distribution of CH25H and PAR1 within astrocytes, 1 cm spinal segments surrounding the lesion sites at 0, 1, 4, and 7 days following SCI were harvested from three rats at each time point for each group. After post-fixing with 4% paraformaldehyde, the cord tissues were cryosectioned into 12μm sections, followed by immunofluorescence staining with the following primary antibodies overnight at 4°C: CH25H (rabbit, 1:100, Invitrogen, Cat# PA5-70691, RRID: AB_2689560); PAR1 (mouse, 1:100, Abcam, Cambridge, UK, Cat# ab233741, RRID: AB_2909530); ionized calcium-binding adaptor molecule-1 (IBA-1) (rabbit, 1:1000, Wako, Richmond, VA, USA, Cat# 019-19741, RRID: AB_839504), GFAP (mouse, 1:400, Sigma, Cat# G3893, RRID: AB_477010), GFAP (rabbit, 1:400, CST, Cat# 80788S, RRID: AB_2799963), or S100β (mouse, 1:400, Abcam, Cambridge, UK, Cat# ab218515, RRID: AB_2868590). Then they were incubated with one of the following secondary antibodies overnight at 4°C: Cy3-labeled goat anti-rabbit IgG (1:400, Proteintech, Chicago, IL, USA, Cat# SA00009-2, RRID: AB_2890957) or Alexa Fluor 488-labeled donkey anti-mouse IgG (1:400, Abcam, Cambridge, UK, Cat# ab150105, RRID: AB_2732856). Images were taken using a fluorescence microscope (Axio Image M2, ZAISS, Shanghai, China). The number of CH25H- or PAR1-positive astrocytes ($CH25H^+GFAP^+$ or $PAR1^+GFAP^+$) per total GFAP-positive ($GFAP^+$) cells was quantified in sections from three rats.

Transwell migration assay

To examine the effects of thrombin-induced production of oxysterol 25-HC on macrophages, macrophage migration was assayed with a 24-well 8-μm Transwell chamber (Costar, Cambridge, MA, USA). Briefly, the astrocytes were treated with 1 U/mL thrombin for 24 hours with or without knockdown of CH25H expression for 48 hours, and the conditioned culture medium (ACM) was then collected to examine its effect on macrophage migration. Alternatively, the astrocytes were treated with 1 U/mL thrombin with or without 100 nM liver X receptor (LXR) antagonist (GSK2033, MCE) or 100 nM LXR agonist (T0901317, MCE) for 24 hours, and the ACM was collected for use in the migration assay. A total of 2×10^4 RAW264.7 cells suspended in 100 μL serum-free DMEM were added to the top chamber of the Transwell system, and the lower chamber was filled with 500 μL of ACM. After incubation for 24 hours at 37°C and 5% CO_2, the cells in the lower chamber were stained with 0.1% crystal violet for 30–45 minutes at 23 ± 2°C. They were then imaged and counted using a DMR inverted microscope (Leica Microsystems, Bensheim, Germany). Assays were performed in triplicate.

Cell viability assay

To test the cell toxicity of the various drugs, astrocytes were seeded in 96-well plates at a density of 6000 cells/well and cultured in an incubator at 37°C and 5% CO_2. The cells were treated with different concentrations of Argatroban, SCH79797, tcY-NH_2, or 25-HC (Simga, Shanghai, China) for 24 hours. After discarding the culture medium in the 96-well plate, 100 μL of 3-(4,5)-dimethylthiahiazo(-z-y1)-3,5-di-phenytetrazoliumromide (MTT) working solution (MTT:serum-free DMEM = 1:9) was added to each well in the dark, and the plates were incubated in a 37°C incubator for 4–6 hours. Then, 100 μL of 20% sodium dodecyl sulfate solution was added, and the plates were incubated for another 20 hours. Absorbance values were measured at 570 nm with a multifunctional enzyme marker (Biotek Synergy2).

Hematoxylin-eosin staining

To assess the size of the lesioned area of spinal cord, 1 cm segments surrounding the lesion sites at T9 were harvested from rats 21 days following SCI, post-fixed, and sectioned. Next, the sections were incubated with hematoxylin and eosin, following standard procedures. Then, the sections were observed under a fluorescence microscope (Axio Image M2, ZAISS). Cells that reacted positively with specific antibodies and lesion areas that stained with hematoxylin-eosin before or after drug treatment were quantified by three investigators using ImageJ v1.8.0 software (National Institutes of Health, Bethesda, MD, USA).

Behavioral tests

Basso-Beattie-Bresnahan (BBB) motor function scores were used to evaluate hindlimb motor function (Zhou et al. 2018). Briefly, hindlimb function while walking was observed and recorded at 0, 7, 14, and 21 days after surgery. In the first stage (0–7 points), hindlimb joint activity was scored. In the second stage (8–13 points), hindlimb gait and the coordination were scored. In the third stage (14–21 points), fine claw movements were scored. The scores for the three stages were combined for a total of 21 possible points. A score of 21 indicated a rat with normal mobility. Successful induction of SCI resulted in a post-operative score of 0.

Statistical analysis

No statistical methods were used to predetermine sample sizes. However, our sample sizes were similar to those reported in a previous publication (Ji et al., 2021). No animals or data points were excluded from the analysis. The assessors were blinded to the groupings in all assays except for immunofluorescence staining. Three sections from each of three animals were assessed for statistical analysis, which was carried out using GraphPad Prism v8.0.2 software (GraphPad Software, San Diego, CA, USA, www.graphpad.com). Comparisons between the two groups were performed using independent sample *t*-test. One-way analysis of variance followed by Bonferroni's *post hoc* comparisons tests was used for mutiple-group comparisons. Results are reported as mean ± standard error of mean (SEM). Statistical significance was defined as $P < 0.05$.

Results

Changes in CH25H expression and its correlation with thrombin activation following SCI in a rat model

To explore whether CH25H expression correlates with thrombin activation at the lesion site following SCI, we used ELISA to determine the levels of thrombin protein in spinal cord segments. The results showed that thrombin expression at lesion sites was increased at 1 and 4 days following SCI in a rat model compared with that in the control and returned to normal levels at 7 days (**Figure 1A** and **B**). Furthermore, *ch25h* expression was increased at 1, 4, and 7 days following SCI compared with that in the control, while *cyp27a1* expression was increased only at 4 and 7 days (**Figure 1C–E**). Treating the lesion site with 4.5 μL of 5 mM SCH79797 (a PAR1 inhibitor) resulted in a marked decrease in ch25h expression compared with treatment with vehicle (**Figure 1C–E**). These findings suggest that thrombin is associated with the regulation of CH25H expression following SCI.

To ascertain whether the astrocytes are involved in thrombin-mediated cholesterol metabolism, immunostaining was performed to detect the cellular distribution of CH25H. The results demonstrated that co-localization of CH25H/GFAP- (**Figure 2A–H**) and CH25H/S100β-positive astrocytes (**Figure 2I–P**) was more frequent at 1, 4, and 7 days following SCI in a rat model compared with 0 day (**Figure 2Q** and **R**). Because thrombin

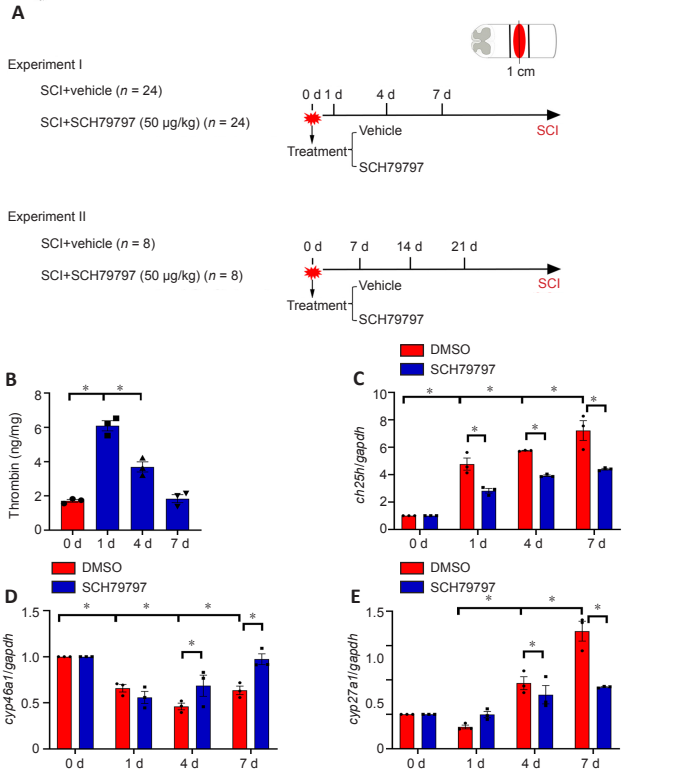

Figure 1 | **Quantitative changes in thrombin production and cholesterol hydroxylase expression at the lesion site following spinal cord injury (SCI) in a rat model.**
(A) Experimental design. Experiment I was designed to investigate the effects of the protease-activated receptor 1 (PAR1) inhibitor SCH79797 on thrombin-induced cholesterol-25-hydroxylase (CH25H) expression by astrocytes. For quantitative polymerase chain reaction, enzyme-linked immunosorbent assay, tissue immunofluorescence, and hematoxylin-eosin staining, 1 cm spinal cord segments were harvested from rats at each time point. Experiment II was designed to investigate the effects of rat motor function after SCH79797 treatment. (B) Enzyme-linked immunosorbent assay of thrombin production at 0, 1, 4, and 7 days following SCI. Day 0 was used as the control. (C–E) RNA levels of *ch25h*, *cyp46a1*, and *cyp27a1* at the lesion site were determined by quantitative polymerase chain reaction at different time points with or without injection of 4.5 μL of 5 mM SCH79797. Quantities were normalized to gapdh levels on day 0. Data are expressed as mean ± SEM (n = 3). *P < 0.05 (independent sample t-test). DMSO: Dimethyl sulfoxide; gapdh: glyceraldehyde-3-phosphate dehydrogenase.

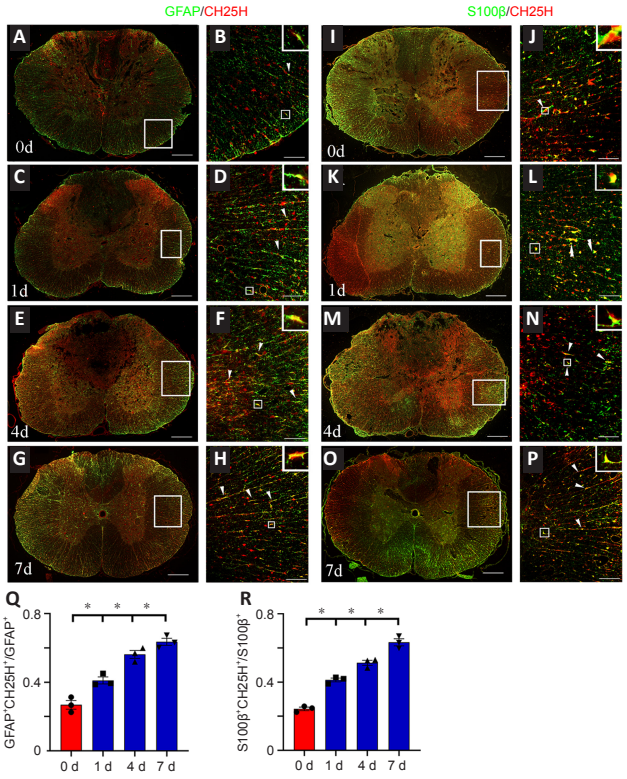

Figure 2 | **Cholesterol-25-hydroxylase (CH25H) colocalization with astrocytes at the lesion site following spinal cord injury (SCI) in a rat model.**
(A–P) Immunostaining showed colocalization of CH25H (Cy3-labeled goat anti-rabbit IgG, red) with glial fibrillary acid protein (GFAP)- (Alexa Fluor 488-labeled donkey anti-mouse IgG, green) and S100β- (Alexa Fluor 488-labeled donkey anti-mouse IgG, green) positive astrocytes. CH25H expression within GFAP- (A–H) and S100β-positive astrocytes (I–P) was significantly increased at 1, 4, and 7 days following SCI. The rectangle indicates the magnified region. Arrowheads indicate positive signals. (Q) Quantification of the ratio of $CH25H^+GFAP^+$-cells to $GFAP^+$-positive cells. (R) Quantification of the ratio of $CH25H^+S100\beta^+$-cells to $S100\beta^+$-positive cells. Scale bars: 500 μm in A, C, E, G, I, K, M, and O; 50 μm in B, D, F, H, J, L, N, and P. Data are expressed as mean ± SEM (n = 3). *P < 0.05 (one-way analysis of variance followed by Bonferroni's *post hoc* comparison test).

mediates cell signaling through PAR1, PAR3, and/or PAR4 (Russell, 2003; Wang et al., 2019b), we next examined the expression of these receptors *par1* was expressed at higher levels in the cord tissue than *par3* and *par4* (**Figure 3A** and **B**). Immunostaining analysis detected PAR1 in GFAP-positive astrocytes before and after SCI (**Figure 3C–F** and **K**), and CH25H expression was significantly decreased in the SCH79797 group compared with that in the control group (**Figure 3G–J** and **L**). These findings suggest that CH25H expression in astrocytes is regulated by the thrombin/PAR1 axis in response to SCI.

Thrombin regulates astrocyte CH25H expression by interacting with PAR1 receptors

To investigate the role of thrombin in the regulation of CH25H expression by astrocytes, we cultured 95% pure primary astrocytes (**Figure 4A**). Adding U/mL thrombin to the astrocytes for 24, 48, or 72 hours induced a rapid elevation in CH25H protein levels in the cells (**Figure 4B**). However, the addition of 5–20 μM of the thrombin inhibitor Argatroban significantly decreased CH25H protein levels, and this effect was not due to cell toxicity (**Figure 4C** and **D**). Next, *par1*, *par3*, and *par4* expression in primary astrocytes was determined by qPCR, and the results were consistent with the *in vivo* results (**Figure 4E**). Western blotting showed that CH25H expression was inhibited in a dose-dependent manner by 0.5–3 μM of the PAR1 inhibitor SCH79797 (**Figure 4F** and **G**). However, siRNA-mediated knockdown of PAR3 expression did not inhibit the thrombin-induced expression of CH25H, similar to the scrambled siRNA control group (**Additional Figure 1A–C**). In contrast, treatment with 100 μM (but not 10 μM) of the PAR4 inhibitor tcY-NH_2 attenuated CH25H expression (**Additional Figure 1D** and **E**). Taken together, these findings indicate that thrombin induces astrocytic expression of CH25H mainly through activation of the PAR1 receptor.

Thrombin promotes the astrocyte CH25H expression through activation of the mitogen-activated protein kinase/NFκB pathway

Thrombin has been shown to affect fibroblasts and macrophages through activation of mitogen-activated protein kinase (MAPK)/NFκB signaling (Chen et al., 2017). To shed light on the signaling pathways involved in thrombin-mediated CH25H expression by astrocytes, the MAPK/NFκB signaling axis was examined in astrocytes treated with thrombin. Western blot analysis showed that stimulating astrocytes with 0.5–2 U/mL thrombin resulted in a significant increase in ERK, JNK, and P38 phosphorylation and NFκB expression compared with a lack of stimulation (**Figure 5A–E**). Adding 0.5–3 μM of the PAR1 inhibitor SCH79797 in the presence of 1 U/mL thrombin markedly inhibited ERK, JNK, and NFκB activation, but not P38 activation, as compared with a lack of SCH79797 treatment (**Figure 5F–J**). We further examined the relevance of MAPK and NFκB activation to astrocyte expression of CH25H using ERK (PD98059), JNK (SP600125), P38 (SB203580), and NFκB (PDTC) inhibitors. The results demonstrated that CH25H expression was significantly attenuated in astrocytes after treatment with 10 μM of the ERK or JNK inhibitor, or 10–100 μM of the NFκB inhibitor, but not 10 μM of the P38 inhibitor, compared with that in astrocytes in the DMSO group (**Figure 6**). These findings indicate that thrombin promotes astrocyte CH25H expression through activation of the ERK- and JNK-mediated NFκB pathway.

Astrocyte-derived 25-HC promotes macrophage migration

To examine the effects of thrombin-induced 25-HC production on macrophages, we added 0-100 μM 25-HC to the culture medium of RAW264.7 macrophages for 24 hours and observed its effects on cell migration. The Transwell assay results demonstrated that treatment of RAW264.7 cells with 5–100 μM 25-HC markedly increased cell migration compared with a lack of treatment (**Additional Figure 2**). Next, astrocytes were treated with 1 U/mL thrombin for 24 hours with or without knockdown of CH25H expression for 48 hours, and the ACM was collected to examine its effect on macrophage migration. The Transwell assay results demonstrated that fewer RAW264.7 in the CH25H siRNA group migrated into the lower chamber compared with those in the scrambled siRNA control group (**Figure 7B**, **D**, and **E**). LXRs are endogenous 25-HC ligands that are very important in the regulation of cholesterol metabolism (Zhao et al., 2020). Adding 100 nM of the LXR antagonist GSK2033 to ACM, significantly reduced RAW264.7 migration in the Transwell assay (**Figure 7A** and **C**), suggesting that GSK2033 abrogates the effects of thrombin-mediated astrocyte 25-HC production on RAW264.7 migration. However, adding 100 nM of T0901317, a highly selective LXR agonist, rescued the inhibitory effects of CH25H knockdown (**Figure 7B** and **E**). These findings indicate that thrombin-induced astrocyte 25-HC production promotes macrophage migration.

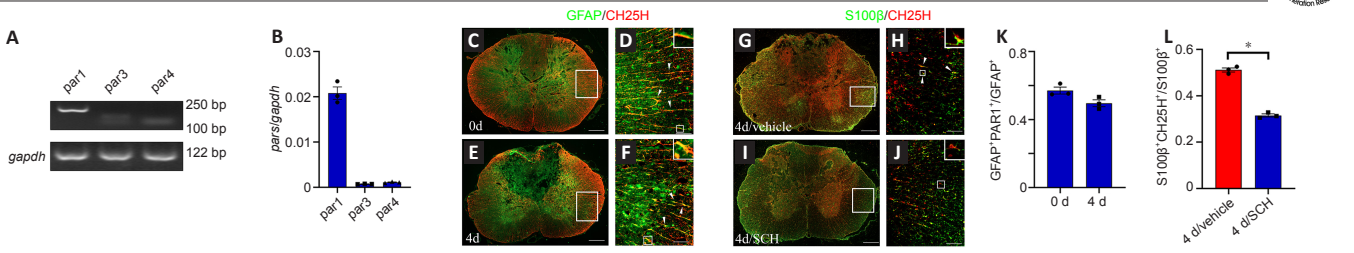

Figure 3 | **Effects of PAR1 inhibition on the astrocyte cholesterol-25-hydroxylase (CH25H) expression following spinal cord injury (SCI) in a rat model.**
(A) Quantitative polymerase chain reaction analysis of *par1*, *par3*, and *par4* expression in spinal cord segments before spinal cord injury. (B) Quantification of *par1*, *par3*, and *par4* expression, normalized to *gapdh*. (C–F) Colocalization analysis of PAR1 (Alexa Fluor 488-labeled donkey anti-mouse IgG, green) with glial fibrillary acid protein (GFAP)- (Cy3-labeled goat anti-rabbit IgG, red) positive astrocytes following SCI at days 0 and 4, showing no difference in PAR1 expression between uninjured and injured cords. (G–J) Immunostaining of CH25H (Cy3-labeled goat anti-rabbit IgG, red) in S100β- (Alexa Fluor 488-labeled donkey anti-mouse IgG, green) positive astrocytes following cord treatment with vehicle (G, H) or the PAR1 inhibitor SCH79797 (I, J) at 4 days. Treatment with SCH79797 significantly decreased the number of CH25H-positive astrocytes. The rectangle indicates the magnified region. Arrowheads indicate positive signals. Scale bars: 500 μm in C, E, G, and I; 50 μm in D, F, H, and J. (K) Quantification of the ratio of $PAR1^+GFAP^+$-cells to $GFAP^+$-positive cells. (L) Quantification of the ratio of $CH25H^+S100\beta^+$-cells to $S100\beta^+$-positive cells. Data are expressed as mean ± SEM (n = 3). *P < 0.05 (independent sample t-test). PAR: Protease-activated receptor.

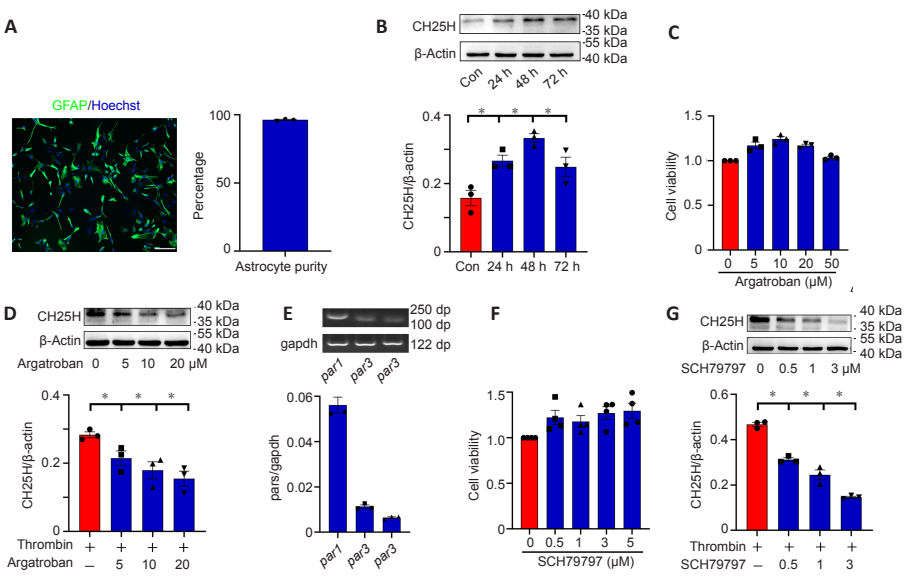

Figure 4 | **Cholesterol-25-hydroxylase (CH25H) expression following treatment of astrocytes with thrombin.**
(A) Primary astrocytes stained with an antibody against glial fibrillary acid protein (GFAP; Alexa Fluor 488-labeled donkey anti-mouse IgG, green) and Hoechst 33342 showing a purity of over 95%. Scale bar: 100 μm. (B) Western blot analysis of CH25H expression following astrocyte stimulation with 1 U/mL thrombin for 24, 48, or 72 hours. Quantities were normalized to β-actin. (C) 3-(4,5)-Dimethylthiahiazo(-z-y1)-3,5-di-phenytetrazoliumromide (MTT) assay of astrocyte viability after stimulation with 0–50 μM argatroban for 24 hours. (D) Western blot analysis of CH25H expression following astrocyte stimulation with 1 U/mL thrombin in the presence or absence of 0–20 μM Argatroban for 24 hours. Quantities were normalized to β-actin. (E) Quantitative polymerase chain reaction analysis of *par1*, *par3*, and *par4* expression in primary astrocytes. Quantities were normalized to *gapdh*. (F) MTT assay of astrocyte viability after stimulation with 0–5 μM SCH79797 for 24 hours. (G) Western blot analysis of CH25H following astrocyte stimulation with 1 U/mL thrombin in the presence or absence of 0–3 μM SCH79797 for 24 hours. Quantities were normalized to β-actin. Data are expressed as mean ± SEM (n = 3). *P < 0.05 (one-way analysis of variance followed by Bonferroni's *post hoc* comparison test). PAR: Protease-activated receptor; SCH79797: PAR1 inhibitor.

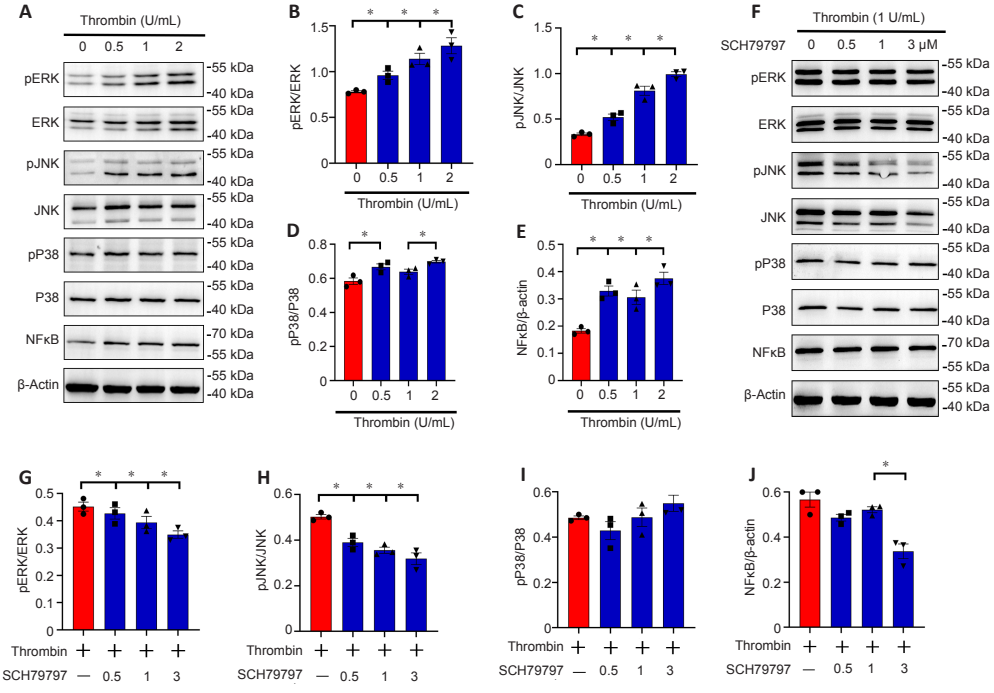

Figure 5 | **Effects of thrombin/protease-activated receptor 1 on the mitogen-activated protein kinase (MAPK)/nuclear factor kappa-B (NFκB) pathway in astrocytes.**
(A) Western blot analysis of phosphorylated extracellular regulated protein kinase (ERK), c-Jun N-terminal kinase (JNK), P38 kinase (P38), and NFκB protein levels following astrocyte stimulation with 0, 0.5, 1, or 2 U/mL thrombin for 24 hours. (B–E) Quantification of phosphorylated ERK, JNK, P38, and NFκB protein levels, normalized to β-actin. (F) Western blot analysis of phosphorylated ERK, JNK, P38, and NFκB protein levels following astrocyte stimulation with 1 U/mL thrombin in the presence of 0–3 μM SCH79797 for 24 hours. (G–J) Quantification of phosphorylated ERK, JNK, P38, and NFκB protein levels, normalized to β-actin. Data are expressed as mean ± SEM (n = 3). *P < 0.05 (one-way analysis of variance followed by Bonferroni's *post hoc* comparison test). SCH79797: Protease-activated receptor 1 inhibitor.

Inhibiting thrombin expression promotes functional recovery after SCI

To assess the therapeutic effect of thrombin blockade after SCI, we used BBB motor function scores to assess motor function after SCI. Because thrombin-induced astrocyte 25-HC production is associated with the migration of innate immune cells (Chen et al., 2017; Zhu et al., 2019), we quantified the microglia/macrophages at the lesion site before or after SCI. The number of IBA-1-positive microglia at the lesion 4 days after SCI was significantly increased in comparison with 0 day (**Figure 8A–D** and **G**), whereas administration of 4.5 μL of a 5 mM solution of the PAR1 inhibitor SCH79797 reduced the number of IBA-1-positive microglia compared with lack of administration (**Figure 8E–G**).

We further examined the effects of inhibiting microglia migration on the size of the lesion. Observation of hematoxylin-eosin staining sections revealed that the lesioned area of the cord in SCH79797 group was significantly reduced compared with that in the vehicle group at 21 days following contusion (**Figure 8H** and **I**).

Next, BBB scores were used to evaluate rat motor function for 21days after SCI. Compared with a lack of treatment, SCH79797 treatment resulted in higher BBB scores at 7, 14, and 21 days (**Figure 8J**). These findings indicate that inhibiting thrombin improves rat motor function after SCI.

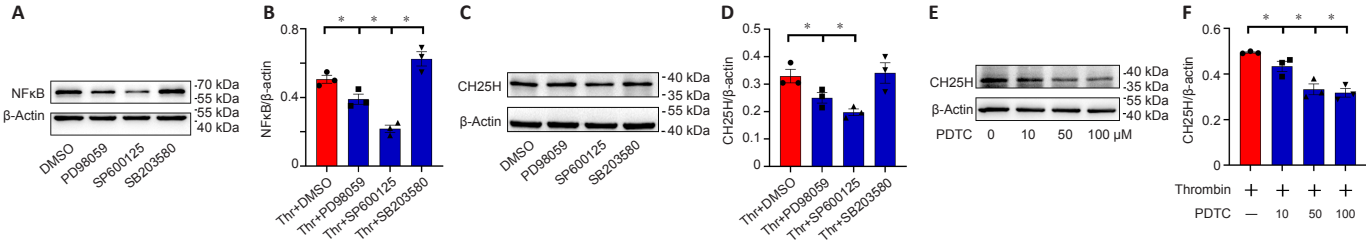

Figure 6 | **Effects of mitogen-activated protein kinase (MAPK) or nuclear factor kappa-B (NFκB) inhibitors on astrocyte cholesterol-25-hydroxylase (CH25H) expression in response to stimulation with thrombin.**

(A) Western blot analysis of NFκB expression following treatment with 1 U/mL thrombin in the presence of 10 μM PD98059, 10 μM SP600125, or 10 μM SB203580 for 24 hours. (B) Quantification of NFκB protein expression, normalized to β-actin. (C) Western blot analysis of CH25H expression following treatment with 1 U/mL thrombin in the presence of 10 μM PD98059, 10 μM SP600125, or 10 μM SB203580 for 24 hours. (D) Quantification of CH25H expression, normalized to β-actin. (E) Western blot analysis of CH25H expression following treatment with 1 U/mL thrombin in the presence or absence of 10–100 μM of the NFκB inhibitor PDTC for 24 hours. (F) Quantification of CH25H expression, normalized to β-actin. Data are expressed as mean ± SEM (n = 3). *P < 0.05 (one-way analysis of variance followed by Bonferroni's *post hoc* comparison test). DMSO: Dimethyl sulfoxide; PD98059: extracellular regulated protein kinases inhibitor; SB203580: P38 inhibitor; SP600125: c-Jun N-terminal kinase inhibitor.

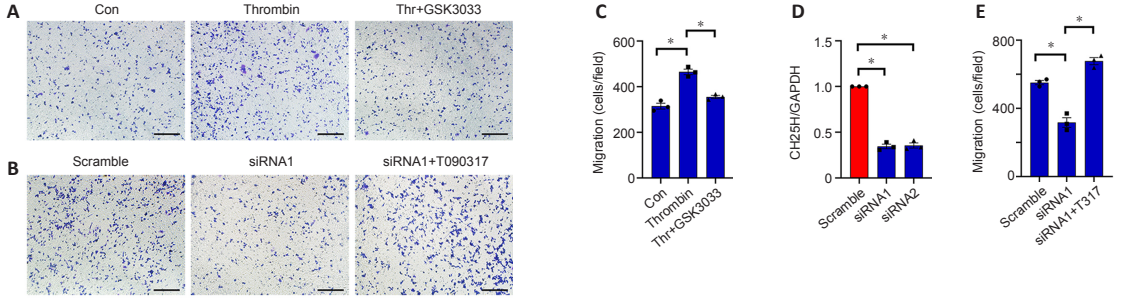

Figure 7 | **Effects of thrombin-induced production of oxysterol 25-hydroxycholesterol (25-HC) on macrophages.**

(A) The Transwell migration assay of RAW264.7 cells cultured with ACM from astrocytes stimulated with 1 U/mL thrombin (Thr) for 24 hours, followed by the addition of 100 nM GSK2033, and allowed to migrate for 24 hours. Treatment with GSK2033 significantly inhibited the effects of thrombin-induced 25-HC expression on RAW264.7 cell migration. (B) The Transwell migration assay of RAW264.7 cells cultured with ACM from astrocytes treated with 1 U/mL thrombin for 24 hours with or without knockdown of cholesterol-25-hydroxylase (CH25H) expression for 48 hours, followed by the addition of 100 nM T0901317, and allowed to migrate for 24 hours. The addition of T0901317 markedly rescued the inhibitory effects of CH25H knockdown on RAW264.7 cell migration. Scale bars: 100 μm. (C) Quantification of RAW264.7 cell migration shown in A. (D) The efficiency of ch25h knockdown was measured by quantitative polymerase chain reaction, with protein expression levels normalized to gapdh. (E) Quantification of RAW264.7 cell migration shown in (B). Data are expressed as mean ± SEM (n = 3). *P < 0.05 (one-way analysis of variance followed by Bonferroni's *post hoc* comparison test). ACM: Conditioned culture medium; Con: Control; GSK2033: liver X receptor antagonist; siRNA: small interfering RNA; T0901317: liver X receptor agonist; Thr: thrombin.

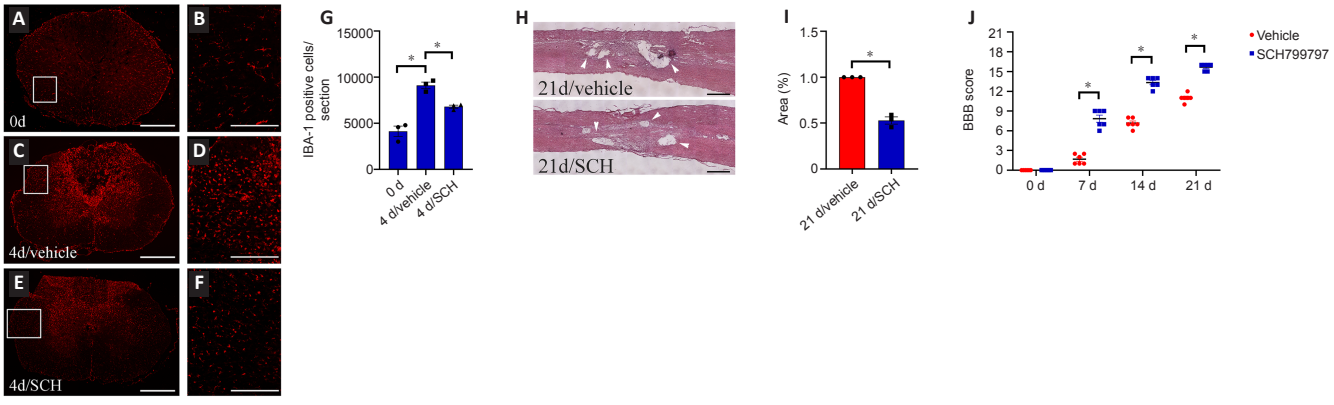

Figure 8 | **Effects of SCH79797 on the recovery of motor function following spinal cord injury (SCI) in a rat model.**

(A–F) Immunostaining of ionized calcium-binding adaptor molecule-1 (IBA-1)- (Cy3-labeled goat anti-rabbit IgG, red) positive microglia following SCI at 0 day (A, B) and 4 day when treated with vehicle (C, D) or the PAR1 inhibitor SCH79797 (E, F). Treatment with SCH79797 significantly reduced the number of IBA-1 positive microglia at the lesion site compared with lack of treatment. The rectangle indicates the magnified region. (G) Quantification of microglia per section. Data are expressed as mean ± SEM (n = 3). (H) Hematoxylin-eosin staining of the injured spinal cord 21 days after injection of 4.5 μL of 5 mM SCH79797 or vehicle at lesion sites. Treatment with SCH79797 decreased the size of the lesion compared with lack of treatment. Arrowheads indicate the cystic cavity. Scale bars: 500 μm in A, C, and E; 50 μm in B, D, and F; 100 μm in H. (I) Quantification of lesion size. Data are expressed as mean ± SEM (n = 3). (J) BBB score for hindlimbs at 0, 7, 14, and 21 days following intrathecal injection of 4.5 μL of 5 mM SCH79797 or vehicle at the lesion site. Data are expressed as mean ± SEM (n = 6). *P < 0.05 (one-way analysis of variance followed by Bonferroni's *post hoc* comparison test for B or independent sample t-test for C). BBB: Basso-Beattie-Bresnahan; PAR: protease-activated receptor; SCH: SCH79797; SCH79797: protease-activated receptor 1 inhibitor.

Discussion

SCI interrupts the connections between axons and peripheral organs, resulting in the paraplegia or quadriplegia. New technologies are being used to help the damage done by SCI, such as the application of polymer scaffolds (Zhang et al., 2019; Luo et al., 2021). However, complete functional recovery and spinal cord regeneration remain elusive. Identifying new players in aberrant CNS cholesterol metabolism is important for understanding the neuropathology of SCI. Cholesterol metabolism is strictly controlled in the CNS and is separated from the peripheral system by the blood-brain barrier and the blood-spinal cord barrier (Göritz et al., 2002). *In situ* cholesterol biosynthesis and elimination of cholesterol derivatives from the CNS are maintained in a delicate balance to prevent the development of a variety of neurological disorders (Hartmann et al., 2021; Jahn et al., 2021; Pikuleva and Cartier, 2021). Several lines of evidence have shown that the different cholesterol derivatives play different neuropathological roles. For example, 24S-hydroxycholesterol (24S-HC), an endogenous positive N-methyl-D-aspartate receptor modulator, participates in N-methyl-D-aspartate receptor mediated neuronal excitotoxicity. However, 25-HC can antagonize 24S-HC potentiation by partially rescuing oxygen and glucose deprivation mediated cell death (Sun et al., 2017). 24S-HC levels have been found to be slightly reduced in the plasma of patients with multiple sclerosis compared with those in healthy individuals, reflecting the loss of brain mass over time (Papassotiropoulos et al., 2000; Leoni and Caccia, 2011). Conversely, elevated blood-derived 27-hydroxycholesterol is found in the cerebrospinal fluid of patients with multiple sclerosis, reflecting blood-brain barrier dysfunction (Leoni and Caccia, 2013). In the present study, we showed that thrombin-mediated 25-HC production is involved in macrophage chemotaxis, consistent with its previously reported proinflammatory function (Gold et al., 2012; Pokharel et al., 2019). Our results provide further evidence for the important role of CH25H in mediating neuroinflammation.

25-HC regulates cell events mainly through binding with two distinct receptor families: nuclear receptor transcription factor LXR and G protein-coupled seven transmembrane domain receptor Epstein-Barr virus-induced gene 2 (EBI2). 25-HC promotes monocyte migration, suppress myelin gene expression in peripheral nerves, and dampens the anti-tumor response of dendritic cells in an LXR-dependent manner (Villablanca et al., 2010; Makoukji et al., 2011; Eibinger et al., 2013). In addition, 25-HC can act as the most active ligand for EBI2 to guide immune cell migration and regulate inflammatory responses (Cyster et al., 2014). In the present study, we found that thrombin-mediated 25-HC production induced macrophage migration of macrophages an LXR-dependent manner. Whether oxysterol performs a similar role by binding the EBI2 receptor remains unknown.

Following CNS injury, thrombin is activated and plays a procoagulant role by cleaving soluble fibrinogen to release fibrin monomers (Di Cera, 2008). In addition, thrombin activates PAR1, PAR3, and PAR4 receptor expression in nerve cells, which modulates the progression of neuropathology (Kim et al., 2021). Previous studies have shown that thrombin activates the astrocytic reaction by influencing morphology, promoting astrogliosis, and enhancing inflammation (Niego et al., 2011; Radulovic et al., 2016). Several investigations have also shown that injury-induced thrombin activation is associated with inhibition of cholesterol biosynthesis, which decreases neurite outgrowth and functional recovery following SCI (Citron et al., 2016; Raghavan et al., 2018; Triplet et al., 2021). Here, we demonstrated that thrombin promotes production of the cholesterol derivative 25-HC by upregulating CH25H expression in astrocytes, suggesting a general role for the serine protease in mediating cholesterol metabolism in various cell types following SCI.

Astrocytes respond to thrombin stimulation by activating multiple intracellular signaling cascades via interactions with PAR1, PAR3, and/or PAR4 (Chen et al., 2022). PAR1, which is a G protein coupled receptor, regulates Ras homolog gene family member A, which in turn catalytically activates phosphoinositide-phospholipase Cε (Dusaban et al., 2013). The phosphoinositide-phospholipase Cε then mediates more sustained activation of protein kinase D and nuclear translocation of NFκB, thus contributing to the pathophysiological roles of astrocytes (Dusaban et al., 2015). Alternatively, the thrombin has been shown to activate MAPK, thereby modulating astrocyte activity, in response to CNS injury (Nicole et al., 2005; Chen et al., 2022). In the present study, we demonstrated that thrombin induces astrocyte CH25H expression through activation of the ERK- and JNK-mediated NFκB pathway, suggesting the importance of the thrombin-activated MAPK/NFκB pathway in the regulation of a variety of astroglial functions following CNS injury.

In conclusion, our results reveal a new regulatory mechanism for aberrant astrocyte cholesterol metabolism that could be beneficial for controlling neuropathology following SCI. A limitation of this study is that we did not determine how much 25-HC was produced by astrocytes stimulated with thrombin.

Author contributions: *Study design and manuscript draft: AG; experiment implementation: CC, HJ; data analysis: CC, HJ, NJ, YjieW, YZ, ZZ, YH, YjunW, AL, AG; manuscript revision: AG, YZ. All authors have approved the present version of the manuscript and have agreed to be accountable for all aspects of the work regarding questions related to the accuracy or integrity of any part of the work.*

Conflicts of interest: *The authors have declared that no competing interests exist.*

Availability of data and materials: *All data generated or analyzed during this study are included in this published article and its supplementary information files.*

Open peer reviewers: *Naomi L. Sayre, University of Texas Health Science Center at San Antonio, USA; Ernesto Doncel-Pérez, National Hospital for Paraplegics, Spain.*

Additional files:

Additional Figure 1: *CH25H expression following astrocytes incubation with thrombin in the presence or absence of various inhibitors.*

Additional Figure 2: *Effects of oxysterol 25-HC on the cell events of macrophages.*

Additional file 1: *Open peer review reports 1 and 2.*

References

Bae JS, Yang L, Manithody C, Rezaie AR (2007) The ligand occupancy of endothelial protein C receptor switches the protease-activated receptor 1-dependent signaling specificity of thrombin from a permeability-enhancing to a barrier-protective response in endothelial cells. Blood 110:3909-3916.

Bauman DR, Bitmansour AD, McDonald JG, Thompson BM, Liang G, Russell DW (2009) 25-Hydroxycholesterol secreted by macrophages in response to Toll-like receptor activation suppresses immunoglobulin A production. Proc Natl Acad Sci U S A 106:16764-16769.

Bensinger SJ, Tontonoz P (2008) Integration of metabolism and inflammation by lipid-activated nuclear receptors. Nature 454:470-477.

Brayton CF (1986) Dimethyl sulfoxide (DMSO): a review. Cornell Vet 76:61-90.

Burda JE, Radulovic M, Yoon H, Scarisbrick IA (2013) Critical role for PAR1 in kallikrein 6-mediated oligodendrogliopathy. Glia 61:1456-1470.

Castrillo A, Joseph SB, Marathe C, Mangelsdorf DJ, Tontonoz P (2003) Liver X receptor-dependent repression of matrix metalloproteinase-9 expression in macrophages. J Biol Chem 278:10443-10449.

Chehrehasa F, Cobcroft M, Young YW, Mackay-Sim A, Goss B (2014) An acute growth factor treatment that preserves function after spinal cord contusion injury. J Neurotrauma 31:1807-1813.

Chen L, Zhang L, Xian G, Lv Y, Lin Y, Wang Y (2017) 25-Hydroxycholesterol promotes migration and invasion of lung adenocarcinoma cells. Biochem Biophys Res Commun 484:857-863.

Chen X, Zhang H, Hao H, Zhang X, Song H, He B, Wang Y, Zhou Y, Zhu Z, Hu Y, Wang Y (2022) Thrombin induces morphological and inflammatory astrocytic responses via activation of PAR1 receptor. Cell Death Discov 8:189.

Citron BA, Ameenuddin S, Uchida K, Suo WZ, SantaCruz K, Festoff BW (2016) Membrane lipid peroxidation in neurodegeneration: Role of thrombin and proteinase-activated receptor-1. Brain Res 1643:10-17.

Coughlin SR (2000) Thrombin signalling and protease-activated receptors. Nature 407:258-264.

Coughlin SR (2005) Protease-activated receptors in hemostasis, thrombosis and vascular biology. J Thromb Haemost 3:1800-1814.

Cyster JG, Dang EV, Reboldi A, Yi T (2014) 25-Hydroxycholesterols in innate and adaptive immunity. Nat Rev Immunol 14:731-743.

Di Cera E (2008) Thrombin. Mol Aspects Med 29:203-254.

Diesch TJ, Mellor DJ, Johnson CB, Lentle RG (2009) Electroencephalographic responses to tail clamping in anaesthetized rat pups. Lab Anim 43:224-231.

Dusaban SS, Kunkel MT, Smrcka AV, Brown JH (2015) Thrombin promotes sustained signaling and inflammatory gene expression through the CDC25 and Ras-associating domains of phospholipase Cε. J Biol Chem 290:26776-26783.

Dusaban SS, Purcell NH, Rockenstein E, Masliah E, Cho MK, Smrcka AV, Brown JH (2013) Phospholipase C epsilon links G protein-coupled receptor activation to inflammatory astrocytic responses. Proc Natl Acad Sci U S A 110:3609-3614.

Eibinger G, Fauler G, Bernhart E, Frank S, Hammer A, Wintersperger A, Eder H, Heinemann A, Mischel PS, Malle E, Sattler W (2013) On the role of 25-hydroxycholesterol synthesis by glioblastoma cell lines. Implications for chemotactic monocyte recruitment. Exp Cell Res 319:1828-1838.

Ferris HA, Perry RJ, Moreira GV, Shulman GI, Horton JD, Kahn CR (2017) Loss of astrocyte cholesterol synthesis disrupts neuronal function and alters whole-body metabolism. Proc Natl Acad Sci U S A 114:1189-1194.

Forwell AL, Bernales CQ, Ross JP, Yee IM, Encarnacion M, Lee JD, Sadovnick AD, Traboulsee AL, Vilariño-Güell C (2016) Analysis of CH25H in multiple sclerosis and neuromyelitis optica. J Neuroimmunol 291:70-72.

Fu H, Zhao Y, Hu D, Wang S, Yu T, Zhang L (2020) Depletion of microglia exacerbates injury and impairs function recovery after spinal cord injury in mice. Cell Death Dis 11:528.

Gold ES, Ramsey SA, Sartain MJ, Selinummi J, Podolsky I, Rodriguez DJ, Moritz RL, Aderem A (2012) ATF3 protects against atherosclerosis by suppressing 25-hydroxycholesterol-induced lipid body formation. J Exp Med 209:807-817.

Göritz C, Mauch DH, Nägler K, Pfrieger FW (2002) Role of glia-derived cholesterol in synaptogenesis: new revelations in the synapse-glia affair. J Physiol Paris 96:257-263.

Grand RJ, Turnell AS, Grabham PW (1996) Cellular consequences of thrombin-receptor activation. Biochem J 313 (Pt2):353-368.

Hartmann H, Ho WY, Chang JC, Ling SC (2021) Cholesterol dyshomeostasis in amyotrophic lateral sclerosis: cause, consequence, or epiphenomenon? FEBS J doi: 10.1111/febs.16175.

Ioannou MS, Jackson J, Sheu SH, Chang CL, Weigel AV, Liu H, Pasolli HA, Xu CS, Pang S, Matthies D, Hess HF, Lippincott-Schwartz J, Liu Z (2019) Neuron-astrocyte metabolic coupling protects against activity-induced fatty acid toxicity. Cell 177:1522-1535.e14.

Jahn T, Clark C, Kerksiek A, Lewczuk P, Lütjohann D, Popp J (2021) Cholesterol metabolites and plant sterols in cerebrospinal fluid are associated with Alzheimer's cerebral pathology and clinical disease progression. J Steroid Biochem Mol Biol 205:105785.

Jayakumar AR, Tong XY, Curtis KM, Ruiz-Cordero R, Shamaladevi N, Abuzamel M, Johnstone J, Gaidosh G, Rama Rao KV, Norenberg MD (2014) Decreased astrocytic thrombospondin-1 secretion after chronic ammonia treatment reduces the level of synaptic proteins: in vitro and in vivo studies. J Neurochem 131:333-347.

Ji H, Zhang Y, Chen C, Li H, He B, Yang T, Sun C, Hao H, Zhang X, Wang Y, Zhou Y, Zhu Z, Hu Y, Li A, Guo A, Wang Y (2021) D-dopachrome tautomerase activates COX2/PGE(2) pathway of astrocytes to mediate inflammation following spinal cord injury. J Neuroinflammation 18:130.

Ju G, Wang J, Wang Y, Zhao X (2014) Spinal cord contusion. Neural Regen Res 9:789-794.

Kim HN, Triplet EM, Radulovic M, Bouchal S, Kleppe LS, Simon WL, Yoon H, Scarisbrick IA (2021) The thrombin receptor modulates astroglia-neuron trophic coupling and neural repair after spinal cord injury. Glia 69:2111-2132.

Lee BB, Cripps RA, Fitzharris M, Wing PC (2014) The global map for traumatic spinal cord injury epidemiology: update 2011, global incidence rate. Spinal Cord 52:110-116.

Leoni V, Caccia C (2011) Oxysterols as biomarkers in neurodegenerative diseases. Chem Phys Lipids 164:515-524.

Leoni V, Caccia C (2013) Potential diagnostic applications of side chain oxysterols analysis in plasma and cerebrospinal fluid. Biochem Pharmacol 86:26-36.

Luo Y, Xue F, Liu K, Li B, Fu C, Ding J (2021) Physical and biological engineering of polymer scaffolds to potentiate repair of spinal cord injury. Mater Des 201:109484.

Maki RA, Tyurin VA, Lyon RC, Hamilton RL, DeKosky ST, Kagan VE, Reynolds WF (2009) Aberrant expression of myeloperoxidase in astrocytes promotes phospholipid oxidation and memory deficits in a mouse model of Alzheimer disease. J Biol Chem 284:3158-3169.

Makoukji J, Shackleford G, Meffre D, Grenier J, Liere P, Lobaccaro JM, Schumacher M, Massaad C (2011) Interplay between LXR and Wnt/β-catenin signaling in the negative regulation of peripheral myelin genes by oxysterols. J Neurosci 31:9620-9629.

Mellor DJ (2010) Galloping colts, fetal feelings, and reassuring regulations: putting animal-welfare science into practice. J Vet Med Educ 37:94-100.

Nicole O, Goldshmidt A, Hamill CE, Sorensen SD, Sastre A, Lyuboslavsky P, Hepler JR, McKeon RJ, Traynelis SF (2005) Activation of protease-activated receptor-1 triggers astrogliosis after brain injury. J Neurosci 25:4319-4329.

Niego B, Samson AL, Petersen KU, Medcalf RL (2011) Thrombin-induced activation of astrocytes in mixed rat hippocampal cultures is inhibited by soluble thrombomodulin. Brain Res 1381:38-51.

Nunomura S, Endo K, Makishima M, Ra C (2010) Oxysterol represses high-affinity IgE receptor-stimulated mast cell activation in liver X receptor-dependent and -independent manners. FEBS Lett 584:1143-1148.

Okada S, Hara M, Kobayakawa K, Matsumoto Y, Nakashima Y (2018) Astrocyte reactivity and astrogliosis after spinal cord injury. Neurosci Res 126:39-43.

Papassotiropoulos A, Lütjohann D, Bagli M, Locatelli S, Jessen F, Rao ML, Maier W, Björkhem I, von Bergmann K, Heun R (2000) Plasma 24S-hydroxycholesterol: a peripheral indicator of neuronal degeneration and potential state marker for Alzheimer's disease. Neuroreport 11:1959-1962.

Patil MJ, Green DP, Henry MA, Akopian AN (2013) Sex-dependent roles of prolactin and prolactin receptor in postoperative pain and hyperalgesia in mice. Neuroscience 253:132-141.

Percie du Sert N, Hurst V, Ahluwalia A, Alam S, Avey MT, Baker M, Browne WJ, Clark A, Cuthill IC, Dirnagl U, Emerson M, Garner P, Holgate ST, Howells DW, Karp NA, Lazic SE, Lidster K, MacCallum CJ, Macleod M, Pearl EJ, et al. (2020) The ARRIVE guidelines 2.0: Updated guidelines for reporting animal research. PLoS Biol 18:e3000410.

Pikuleva IA, Cartier N (2021) Cholesterol hydroxylating cytochrome P450 46A1: from mechanisms of action to clinical applications. Front Aging Neurosci 13:696778.

Pokharel SM, Shil NK, Gc JB, Colburn ZT, Tsai SY, Segovia JA, Chang TH, Bandyopadhyay S, Natesan S, Jones JCR, Bose S (2019) Integrin activation by the lipid molecule 25-hydroxycholesterol induces a proinflammatory response. Nat Commun 10:1482.

Radulovic M, Yoon H, Wu J, Mustafa K, Scarisbrick IA (2016) Targeting the thrombin receptor modulates inflammation and astrogliosis to improve recovery after spinal cord injury. Neurobiol Dis 93:226-242.

Raghavan S, Singh NK, Mani AM, Rao GN (2018) Protease-activated receptor 1 inhibits cholesterol efflux and promotes atherogenesis via cullin 3-mediated degradation of the ABCA1 transporter. J Biol Chem 293:10574-10589.

Rodnight RB, Gottfried C (2013) Morphological plasticity of rodent astroglia. J Neurochem 124:263-275.

Russell DW (2000) Oxysterol biosynthetic enzymes. Biochim Biophys Acta 1529:126-135.

Russell DW (2003) The enzymes, regulation, and genetics of bile acid synthesis. Annu Rev Biochem 72:137-174.

Schwab JM, Zhang Y, Kopp MA, Brommer B, Popovich PG (2014) The paradox of chronic neuroinflammation, systemic immune suppression, autoimmunity after traumatic chronic spinal cord injury. Exp Neurol 258:121-129.

Shibata N, Kawarai T, Meng Y, Lee JH, Lee HS, Wakutani Y, Shibata E, Pathan N, Bi A, Sato C, Sorbi S, Bruni AC, Duara R, Mayeux R, Farrer LA, George-Hyslop PS, Rogaeva E (2007) Association studies between the plasmin genes and late-onset Alzheimer's disease. Neurobiol Aging 28:1041-1043.

Sofroniew MV, Vinters HV (2010) Astrocytes: biology and pathology. Acta Neuropathol 119:7-35.

Sun MY, Taylor A, Zorumski CF, Mennerick S (2017) 24S-hydroxycholesterol and 25-hydroxycholesterol differentially impact hippocampal neuronal survival following oxygen-glucose deprivation. PLoS One 12:e0174416.

Suo Z, Wu M, Ameenuddin S, Anderson HE, Zoloty JE, Citron BA, Andrade-Gordon P, Festoff BW (2002) Participation of protease-activated receptor-1 in thrombin-induced microglial activation. J Neurochem 80:655-666.

Triplet EM, Kim HN, Yoon H, Radulovic M, Kleppe L, Simon WL, Choi CI, Walsh PJ, Dutton JR, Scarisbrick IA (2021) The thrombin receptor links brain derived neurotrophic factor to neuron cholesterol production, resiliency and repair after spinal cord injury. Neurobiol Dis 152:105294.

Tsai HH, Li H, Fuentealba LC, Molofsky AV, Taveira-Marques R, Zhuang H, Tenney A, Murnen AT, Fancy SP, Merkle F, Kessaris N, Alvarez-Buylla A, Richardson WD, Rowitch DH (2012) Regional astrocyte allocation regulates CNS synaptogenesis and repair. Science 337:358-362.

van Deijk AF, Camargo N, Timmerman J, Heistek T, Brouwers JF, Mogavero F, Mansvelder HD, Smit AB, Verheijen MH (2017) Astrocyte lipid metabolism is critical for synapse development and function in vivo. Glia 65:670-682.

Vaya J, Schipper HM (2007) Oxysterols, cholesterol homeostasis, and Alzheimer disease. J Neurochem 102:1727-1737.

Villablanca EJ, Raccosta L, Zhou D, Fontana R, Maggioni D, Negro A, Sanvito F, Ponzoni M, Valentinis B, Bregni M, Prinetti A, Steffensen KR, Sonnino S, Gustafsson JA, Doglioni C, Bordignon C, Traversari C, Russo V (2010) Tumor-mediated liver X receptor-alpha activation inhibits CC chemokine receptor-7 expression on dendritic cells and dampens antitumor responses. Nat Med 16:98-105.

Wang P, Qi X, Xu G, Liu J, Guo J, Li X, Ma X, Sun H (2019a) CCL28 promotes locomotor recovery after spinal cord injury via recruiting regulatory T cells. Aging (Albany NY) 11:7402-7415.

Wang S, Yao Y, Wang X, Zheng G, Ouyang W, Chen W (2019b) 25-HC promotes hepatocellular carcinoma metastasis through up-regulation of TLR4 dependent FABP4. Am J Cancer Res 9:2140-2155.

Whetstone WD, Walker B, Trivedi A, Lee S, Noble-Haeusslein LJ, Hsu JC (2017) Protease-activated receptor-1 supports locomotor recovery by biased agonist activated protein c after contusive spinal cord injury. PLoS One 12:e0170512.

Wong MY, Lewis M, Doherty JJ, Shi Y, Cashikar AG, Amelianchik A, Tymchuk S, Sullivan PM, Qian M, Covey DF, Petsko GA, Holtzman DM, Paul SM, Luo W (2020) 25-Hydroxycholesterol amplifies microglial IL-1β production in an apoE isoform-dependent manner. J Neuroinflammation 17:192.

Yoon J, Choi N, Ko J, Kim K, Lee S, Choo J (2013) Highly sensitive detection of thrombin using SERS-based magnetic aptasensors. Biosens Bioelectron 47:62-67.

Yoshizaki S, Tamaru T, Hara M, Kijima K, Tanaka M, Konno DJ, Matsumoto Y, Nakashima Y, Okada S (2021) Microglial inflammation after chronic spinal cord injury is enhanced by reactive astrocytes via the fibronectin/β1 integrin pathway. J Neuroinflammation 18:12.

Zeng H, Liu N, Yang YY, Xing HY, Liu XX, Li F, La GY, Huang MJ, Zhou MW (2019) Lentivirus-mediated downregulation of α-synuclein reduces neuroinflammation and promotes functional recovery in rats with spinal cord injury. J Neuroinflammation 16:283.

Zhang Q, Shi B, Ding J, Yan L, Thawani JP, Fu C, Chen X (2019) Polymer scaffolds facilitate spinal cord injury repair. Acta Biomater 88:57-77.

Zhao J, Chen J, Li M, Chen M, Sun C (2020) Multifaceted functions of CH25H and 25HC to modulate the lipid metabolism, immune responses, and broadly antiviral activities. Viruses 12:727.

Zhou Y, Guo W, Zhu Z, Hu Y, Wang Y, Zhang X, Wang W, Du N, Song T, Yang K, Guan Z, Wang Y, Guo A (2018) Macrophage migration inhibitory factor facilitates production of CCL5 in astrocytes following rat spinal cord injury. J Neuroinflammation 15:253.

Zhu Z, Hu Y, Zhou Y, Zhang Y, Yu L, Tao L, Guo A, Fang Q (2019) Macrophage migration inhibitory factor promotes chemotaxis of astrocytes through regulation of cholesterol 25-hydroxylase following rat spinal cord injury. Neuroscience 408:349-360.

P-Reviewers: Sayre NL, Doncel-Pérez E; C-Editor: Zhao M; S-Editors: Yu J, Li CH; L-Editors: Crow E, Yu J, Song LP; T-Editor: Jia Y

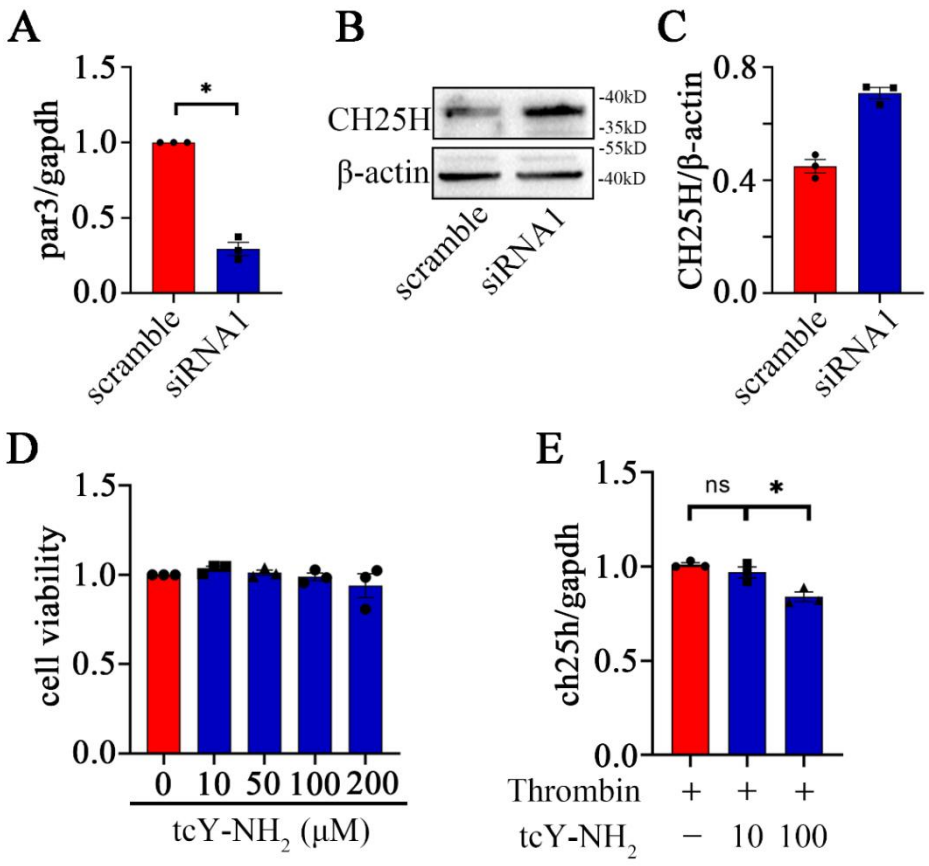

Additional Figure 1 CH25H expression following astrocytes incubation with thrombin in the presence or absence of various inhibitors.

(A) Interference efficiency of siRNA oligonucleotides for *par3* was measured by quantitative polymerase chain reaction. Quantities were normalized to *gapdh* in scramble group. (B) Western blot analysis of CH25H following siRNA knockdown of *par3* for 48 hours, prior to stimulation with 1 U/mL thrombin for 24 hours. Quantities were normalized to β-actin. (C) Quantification of CH25H expression. (D) MTT assay of astrocytes viability after stimulation with 0-200 μM tcY-NH_2 for 24 hours. (E) Transcription of *ch25h* was determined by quantitative polymerase chain reaction, prior to stimulation with 1 U/mL thrombin in the presence or absence of 10-100 μM tcY-NH_2 for 24 hours. Quantities were normalized to *gapdh*. Data are expressed as mean ± SEM (n = 3). *P< 0.05 (independent sample t-test (A, C) or one-way analysis of variance followed by Bonferroni's *post hoc* comparison test (D, E)). CH25H: cholesterol-25-hydroxylase; gapdh: glyceraldehyde-3-phosphate dehydrogenase; par: protease-activated receptor; siRNA: small interfering RNA; tcY-NH_2: protease-activated receptor 4 inhibitor.

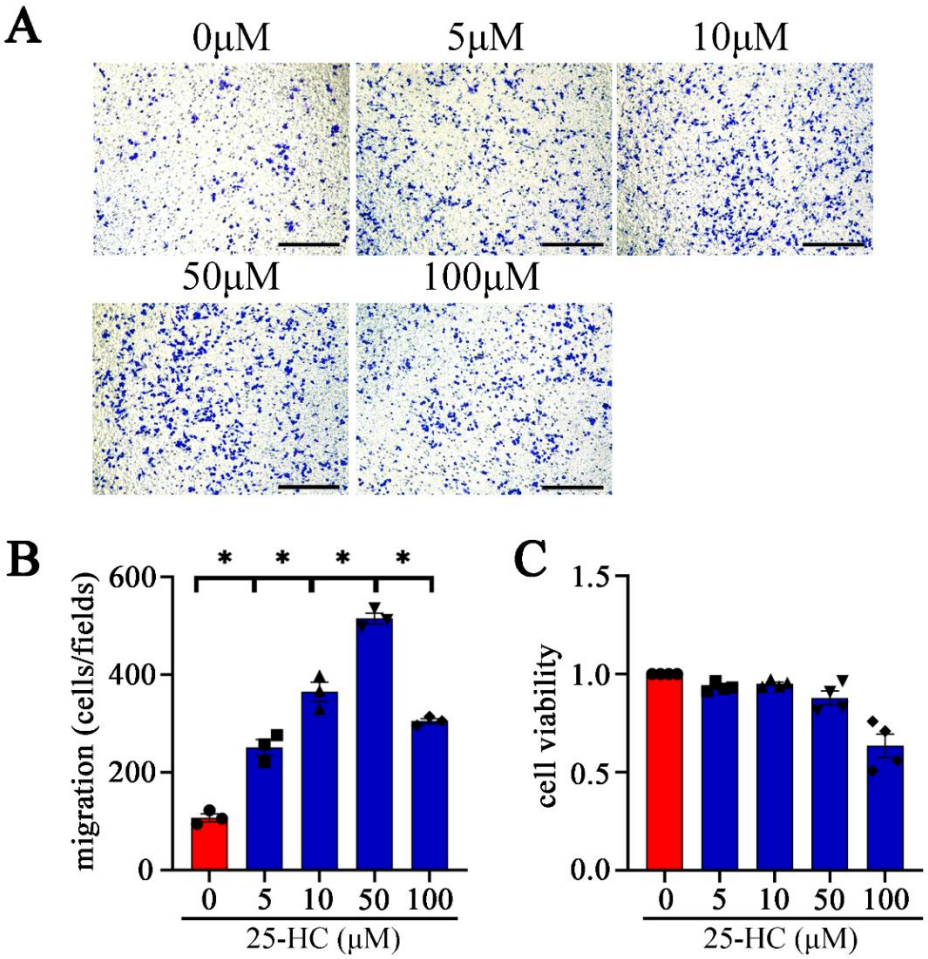

Additional Figure 2 Effects of oxysterol 25-HC on the cell events of macrophages.

(A) The Transwell analysis of the migration of RAW264.7 cells treated with 0-100 μM 25-HC for 24 hours. Treatment of RAW264.7 cells with 5-100 μM 25-HC remarkably facilitated cell migration in comparison with the control. Scale bars: 100 μm. (B) Quantification of RAW264.7 cells. (C) 3-(4,5)-Dimethylthiahiazo(-z-y1)-3,5-di-phenytetrazoliumromide assay of RAW264.7 cells viability after stimulation with 0-100 μM 25-HC for 24 hours. Data are expressed as mean ± SEM (n = 3). *P < 0.05 (one-way analysis of variance followed by Bonferroni's *post hoc* comparison test). 25-HC: 25-Hydroxycholesterol.